Supplementary Information

Controlled modification of skyrmions information in a three-terminal racetrack memory

Kang Wang,[a,b] Lijuan Qian,[b] See-Chen Ying,[b] Gang Xiao,*[b] and Xiaoshan Wu*[1]

Affliations

[a]*Collaborative Innovation Center of Advanced Microstructures, Laboratory of Solid State Microstructures, School of Physics, Nanjing University, Nanjing 210093, China.* E-mail: xswu@nju.edu.cn

[b]*Department of Physics, Brown University, Providence, Rhode Island 02912, USA*. E-mail: gang_xiao@brown.edu

Supplementary Note 1: Current distributions in a three-terminal racetrack memory

In our simulation studies, we employ a model system with parameters corresponding to a bilayer of $Co_{60}Fe_{20}B_{20}$ (0.8 nm)/Pt (2.7 nm). A charge current (J_e) to drive skyrmions to move is applied in the heavy metal layer through the application of a voltage between the generator and the collector. Due to the spin Hall effect in the Pt layer with spin Hall angle $\Theta_{SH} = 0.07$,[1] a corresponding spin current ($J_s e_z$ with $J_s = \Theta_{SH} J_e$) is then injected into the magnetic layer. The spin polarization $m_p = \frac{J_e}{J_e} \times e_z$ is a unit vector perpendicular to the charge current applied in the Pt layer. Current distributions in the Pt layer are calculated (through a two-dimensional model) using the COMSOL multiphysics modelling software. The assumed specific resistivity is $\rho_{Pt} = 12 \times 10^{-8}\ \Omega m$.[2] Normalized charge current density $J_e/J_{e,max}$ in the Pt layer is illustrated in Supplementary Fig. 1. When applying a voltage at the generator (V_G), the current distributes almost uniformly along the wire, leading to a steady motion of skyrmions along the racetrack (Supplementary Fig. 1(a)). During the skyrmions generation or deletion process, in addition to the voltage pulse at the generator, a stronger voltage is also applied at the controller (V_C). Supplementary Fig. 1(b) illustrates the normalized charge current density when the V_G is off. Local stronger current can be found close to the narrow track (Insert in Supplementary Fig. 1(b)). This leads to the reversal of spin states. V_C required to write or delete a skyrmion is larger than V_G by two-orders of magnitude. This means that the on or off state of the voltage pulse at the generator only has a quite small effect on the skyrmions manipulation process. However, we have taken this slight difference into simulations when we study the skyrmions generation and annihilation, to ensure the simulations accuracy.

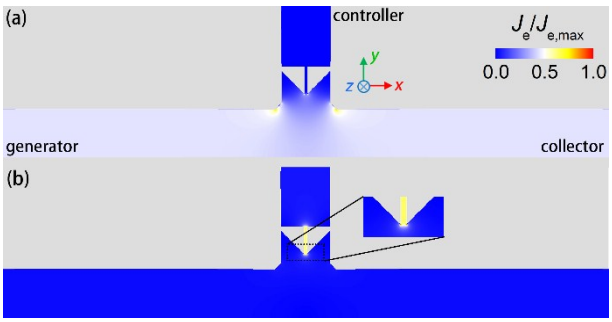

Supplementary Fig. 1 (a) Normalized charge current distributions with the voltage pulse at the generator. The current distributes almost homogeneously over the magnetic nanoribbon, allowing steady motion of skyrmions along the wire. (b) Normalized charge current distributions with the voltage pulse at the controller while both the electric potentials at the generator and collector remain at zero. Local stronger current at the narrow track is obviously observed. This leads to the flip of spin polarization.

From the charge current distributions, the spin current $J_s e_z$ with spin polarization m_p are then calculated (Supplementary Fig. 2). With a positive (Supplementary Fig. 2(b)) or negative (Supplementary Fig. 2(c)) voltage applied at the controller, the spin-current flows along z-axis but with the opposite spin polarization depending on the sign of the voltage applied. This leads to the generation or deletion of a single skyrmion. Accurate current distributions provide a fundamental basis for precise simulations.

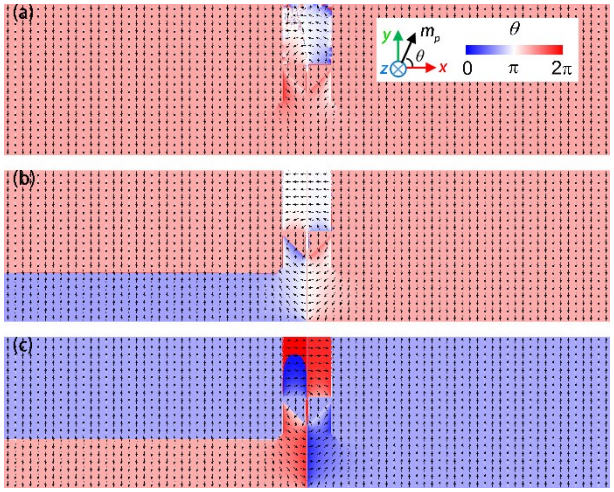

Supplementary Fig. 2 (a) In-plane spin polarization distributions when a voltage is applied at the generator, (b) In-plane spin polarization distributions when a positive voltage is applied at the controller. (c) In-plane spin polarization distributions when a negative voltage is applied at the controller. The spin current flows along the z-axis but with the sign of the spin polarization depending on the sign of applied voltage. This allows diverse spin dynamics around the narrow track. Spin directions outside the three-terminal racetrack memory are not taken into consideration in simulations where the spin current remains zero.

Supplementary Note 2: The steady motion of skyrmions

The centre of mass motion of a skyrmion is described by the Thiele equation (Eq.(3) in the main manuscript). Taking the spin current and boundary repulsions into consideration, the steady state motion of the skyrmion is given by

$$-Gv_y + \alpha D v_x - TRJ_e = 0 \tag{S1}$$

$$Gv_x + \alpha D v_y - \frac{\gamma}{M_S d} F_y = 0. \quad \text{(S2)}$$

Here v_x and v_y are skyrmion velocities along the magnetic wire and perpendicular to it. F_y is the border repulsion. Generally, F_y increases with increasing transverse displacement (y) from the centre of the strip.[3]

Values of v_x and v_y calculated from Eqns. (S1) and (S.2) are shown in Supplementary Fig. 3(a) and (b) with different current density applied. Although the charge current is applied along x-axis, there is still a y-component motion for a skyrmion. This is known as the skyrmion Hall effect that has also been observed in recent experiments.[4] With increasing off-centred displacement, v_y decreases and v_x increases. Calculated v_x and v_y show the same trend as that observed in our micromagnetic simulation. For a particular off-centred displacement Δy, the y-component velocity vanishes due to the balance between SOT and boundary repulsions. This off-centred displacement Δy increases with increasing current (Supplementary Fig. 3(c)). When the current exceeds a critical value, the SOT dominates and the skyrmion would be annihilated upon touching the boundary.

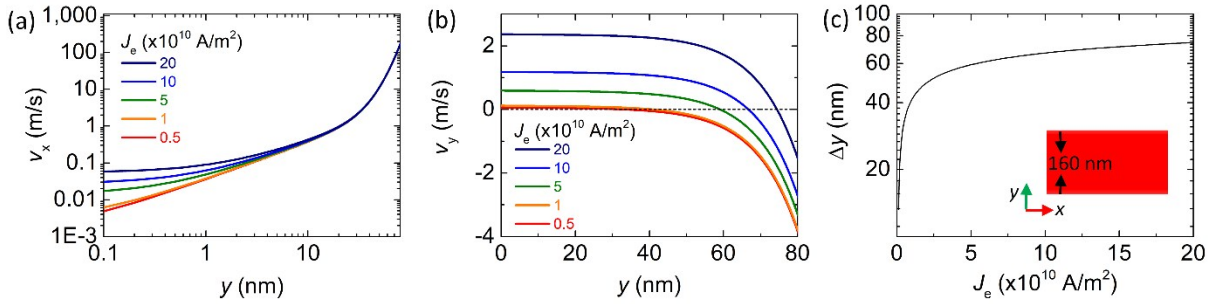

Supplementary Fig. 3 (a) Longitudinal and (b) transverse velocities at different transverse positions with current applied. The centre of the wire (insert of (c)) is assigned to be $y = 0$. Due to the spin-orbit torque, skyrmions move with positive v_x and v_y. v_x increases and v_y decreases when a skyrmion is driven close to the boundary. The trend is the same with our results from micromagnetic simulation studies. From (b), an equilibrium position Δy with $v_y = 0$ is inferred. (c) Δy increases with increasing current. When the current exceeds a critical value, there is no solution for Δy for which $v_y = 0$ and the skyrmion will touch the boundary and then be annihilated.

Supplementary Note 3: The effects of pulse durations on skyrmions motion

When we apply a train of voltage pulses at the generator to drive the skyrmions toward the collector, it is essential to keep skyrmions codes from distortion. In the above discussion, we have shown that the current density and initial off-centred positions for skyrmions are critical factors for achieving steady motion. However, in Supplementary Note 2, we have assumed that a continuous current is applied. In practical experiments, a pulsed current is generally used to avoid overheating. This is the reason why we use the pulsed current to drive skyrmions in the racetrack memory. In this part, we briefly discuss the effects of pulse durations on skyrmions motion.

Both with the continuous current and pulsed current (with pulse duration $\Delta\tau = 3\ ns$ period) applied, time-dependent longitudinal (Supplementary Fig. 4(a)) and transversal (Supplementary Fig. 4(b)) positions show similar results. Constant *y*-coordinates during a large part of the skyrmions trajectory illustrated in Supplementary Fig. 4(b) for both cases further confirm the results shown in Supplementary Fig. 3(c). The short pulse during which the value of the transverse coordinate increases and then resumes the original constant value correspond to time interval when the skyrmion is moving through the controller region. The main difference is that the average velocity in the longitudinal direction is slower for the pulsed driving, resulting from the absence of SOT during the period when the current is off. The comparison between the two circumstances demonstrates that the pulse duration is not an important factor in the driven skyrmions motion.

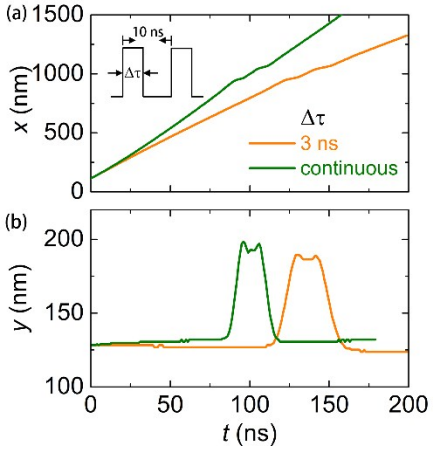

Supplementary Fig. 4 (a) Time-dependent longitudinal and (b) transverse coordinates when we apply a pulsed current with duration of $\Delta\tau = 3\ ns$ (orange lines) and continuous current (green lines) along the three-terminal racetrack memory. Insert in (a) is the diagram of the pulsed current to drive skyrmions move along the racetrack.

Supplementary Note 4: Thiele equation and the coupling of Breathing and Gyration mode

For the time dependent trajectory of a skyrmion, both the centre of mass coordinate $r(t)$ and the skyrmion radius $R(t)$, can be separated into a slowly time varying components $r_0(t)$ and $R_0(t)$ and more rapidly oscillatory components ($\Delta r(t) = \Delta x e_x + \Delta y e_y$ and $\Delta R(t)$). We analyse the Fourier transform of the oscillatory part of $r(t)$ and $R(t)$ as described in Eq.(4) of the main manuscript leading to the equations

$$-\frac{\gamma}{M_S d}M(2\pi)^2\nu^2 A_x^{'}(\nu) + G2\pi\nu A_y^{''}(\nu) - \alpha D2\pi\nu A_x^{''}(\nu) - \beta\varepsilon J_e\frac{\pi^2}{2}\Delta R^{'}(\nu) = 0 \quad \text{(S3a)}$$

$$\frac{\gamma}{M_S d}M(2\pi)^2\nu^2 A_x^{''}(\nu) + G2\pi\nu A_y^{'}(\nu) - \alpha D2\pi\nu A_x^{'}(\nu) + \beta\varepsilon J_e\frac{\pi^2}{2}\Delta R^{''}(\nu) = 0 \quad \text{(S3b)}$$

$$-\frac{\gamma}{M_S d}M(2\pi)^2\nu^2 A_y^{'}(\nu) - G2\pi\nu A_x^{''}(\nu) - \alpha D2\pi\nu A_y^{''}(\nu) + \frac{\gamma}{M_S d}K A_y^{'}(\nu) = 0 \quad \text{(S3c)}$$

$$\frac{\gamma}{M_S d}M(2\pi)^2\nu^2 A_y^{''}(\nu) - G2\pi\nu A_x^{'}(\nu) - \alpha D2\pi\nu A_y^{'}(\nu) - \frac{\gamma}{M_S d}K A_y^{''}(\nu) = 0. \quad \text{(S3d)}$$

We note that there is a $\frac{\pi}{2}$- phase difference between the *x*- and *y*-components of the gyrating motion of a skyrmion. This implies that $A_x^{'} = -A_y^{''}$ and $A_x^{''} = A_y^{'}$ if we assume that $|A_x(\nu)| = \sqrt{A_x^{'2}(\nu) + A_x^{''2}(\nu)}$ is the same as $|A_y(\nu)| = \sqrt{A_y^{'2}(\nu) + A_y^{''2}(\nu)}$. Substituting $A_y^{'}$ and $A_y^{''}$ by $A_x^{''}$ and $-A_x^{'}$ respectively, into Eq.(S3a-d) yields after a little manipulation the result

$$\left[-\frac{\gamma}{M_S d}M(2\pi)^2\nu^2 - G2\pi\nu + i\alpha D2\pi\nu + \frac{\gamma}{2M_S d}K\right]A_x(\nu) - \frac{1}{2}TJ_e\Delta R(\nu) = 0 \quad \text{(S4)}$$

,

where $A_x(\nu) = A_x^{'}(\nu) + iA_x^{''}(\nu)$ and $\Delta R(\nu) = \Delta R^{'}(\nu) + i\Delta R^{''}(\nu)$. This then yields the result

$$A_x(\nu) = \chi(\nu, J_e, K)\Delta R(\nu), A_y(\nu) = -i\chi(\nu, J_e, K)\Delta R(\nu), \quad \text{(S5)}$$

with

$$\chi(\nu, J_e, K) = \frac{\frac{1}{2}TJ_e}{-\frac{\gamma}{M_S d}M(2\pi)^2\nu^2 + 2\pi(-G + i\alpha D)\nu + \frac{\gamma}{2M_S d}K} \quad \text{(S6)}$$

The above equation suggests that the FFT spectrum for the gyration mode is modulated by the breathing mode of a skyrmion. Obviously, $\chi(\nu, J_e, K)$ depends on the inertial mass of a skyrmion, current applied and the repulsive force from the racetrack boundary.

Supplementary Note 5: Repulsive force from the racetrack edge

As presented in the main manuscript, the boundary force F is given as $F = -\partial_r U$ where U is the free energy exactly described in Eq. (2). Thus, from the total energy extracted from micromagnetic simulations, the boundary force and the stiffness $\vec{\vec{K}}$ can be derived (Supplementary Fig. 5). For a skyrmion in a racetrack as inserted in Supplementary Fig. 5(a), the boundary force only has a *y*-component value F_y and $K_{yy} = K$ in the tensor $\vec{\vec{K}}$ remains non-zero. Results show an increasing boundary force with decreasing the distance (y_{sb}) from the skyrmion centre of mass to the racetrack edge. For the particular magnetic parameters adopted in our simulations, F_y is only a function of y_{sb} (Supplementary Fig. 5(a)).

The stiffness K is calculated through $K = \partial_y F_y$ as a spatial derivation of the boundary force (Supplementary Fig. 5(b)). For a skyrmion in a racetrack with the width of $D_w = 160\ nm$, the K value is almost independent of the current. This indicates that the boundary force for a skyrmion located at a fixed position is only determined by the magnetic parameters adopted in micromagnetic simulations studies.

Due to the complex structure of the controller in the three-terminal racetrack, K_{xx}, K_{xy} and K_{yx} are no longer zero. However, when processing the skyrmion dynamics observed during skyrmions generation and annihilation processes, we reduce the $\vec{\vec{K}}$ to be a constant K to simplify the calculation. Even though, the main peak around 8.5 GHz and a small peak around 2.4 GHz in the gyration mode spectrum can still be well simulated from the response function; however, the fitting K may be slightly different from the actual value determined directly from the free energy U.

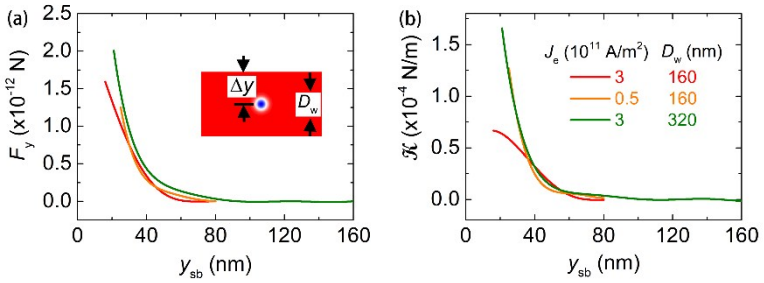

Supplementary Fig. 5 Repulsive force from the racetrack boundary. (a) Boundary force F_y as a function of the distance from the skyrmion centre of mass to the racetrack edge (y_{sb}). Insert is the racetrack with a width of D_w studied in micromagnetic simulations studies. (b) The stiffness K as a function of y_{sb}.

Supplementary Note 6: Inertial mass of a skyrmion

In the response function shown in Eq. (S6), both the inertial mass of a skyrmion and the stiffness $\mathcal{K}$ are needed to describe the gyration mode spectrum which is coupled to the breathing mode dynamics. The boundary force has been discussed in Supplementary Note 5. In order to determine the inertial mass of a skyrmion, we analyse the skyrmion dynamics for a skyrmion in an infinite layer where $K = 0$. When we apply a charge current $J_e e_x$ ($J_e = 3 \times 10^{11}\ A/m^2$, the followings are the same) in the Pt layer, both the oscillatory variation of the skyrmion radius and gyrating motion of the center of mass are observed (Supplementary Fig. 6(a)), from which the FFT spectra of the gyration and breathing modes can be derived (Supplementary Fig. 6(b)). In this case, the inertial mass is the only fitting parameter in Eq. (S6). The best fit of the simulation result with Eq.(S6) results in the value $M \sim 1.46 \times 10^{-24}\ kg$. This inertial mass corresponds to a mass density of $\rho = \frac{M}{2\pi R d} \sim 2.07 \times 10^{-8}\ kg/m^2$ with $R = 14.07\ nm$. In the next section, we demonstrate that the mass density is a more meaningful parameter than the inertial mass in describing the skyrmion dynamics.

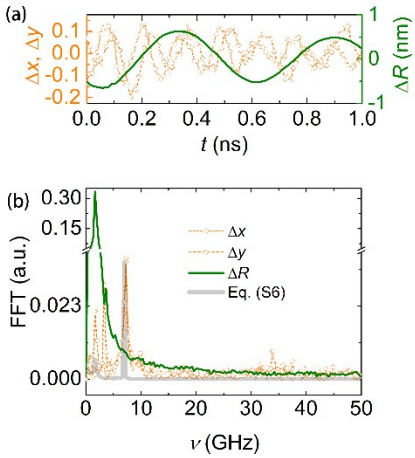

Supplementary Fig. 6 (a) Real-time spectra of breathing and gyration modes for a skyrmion in an infinite layer without boundary force. (b) the fast Fourier transformation (FFT) of the breathing mode (ΔR) for a skyrmion, and trajectories of the centre of mass (Δx and Δy). Gray line is calculated from Eqs. (S6)

Supplementary Note 7: The effects of current and boundary force on skyrmion dynamics

We note that both the breathing (ν_b) and gyration mode (ν_g) frequencies observed during skyrmions generation and deletion are larger than that for a skyrmion in an infinite layer with the charge current $J_e e_x$ applied. We attribute this to the large boundary force with a small distance from the center of mass to the racetrack edge (Supplementary Fig. 6(b)), while the current only has a comparatively small effect on the frequencies (Supplementary Fig. 7(a)). For a skyrmion in an infinite layer without boundary repulsions, the breathing mode frequency decreases when the current increases. If taking the boundary force into account, frequency dependence of the current is even much reduced.

To further demonstrate that the frequency is raised by the boundary force, we look into the dynamics of a skyrmion in a constricted structure with the width of $D_w = 160\ nm$ as illustrated in Supplementary Fig. 7(a). When a skyrmion is located at a position with a large off-centred displacement, a larger $\mathcal{K}$ value results, and both breathing and gyration mode frequencies greatly increase (see Supplementary Fig. 7(b)). We employ Eq. (S6) to calculate the $\mathcal{K}$-dependent gyration mode frequency with a given $M = 1.46 \times 10^{-24}\ kg$. We find that the calculated result does not agree with the results directly from micromagnetic simulations studies. The reason is that the variation of the inertial mass of a skyrmion with its radius need to be taken into account. When a skyrmion is driven from the centre of the racetrack to the position close to the racetrack edge, the skyrmion size decreases from 13.2 nm to sub-10 nm. This leads to

a change of the inertial mass $M = 2\pi\rho Rd$ if we assume the mass density a constant. We obtain the radius of a skyrmion from the micromagnetic simulations. With the corrected inertial mass, the result calculated from the Eq. (S6) reproduces well the K dependence of the gyration mode frequencies. This shows that the inertial mass density is a more meaningful parameter compared with the inertial mass when studying the skyrmion dynamics.

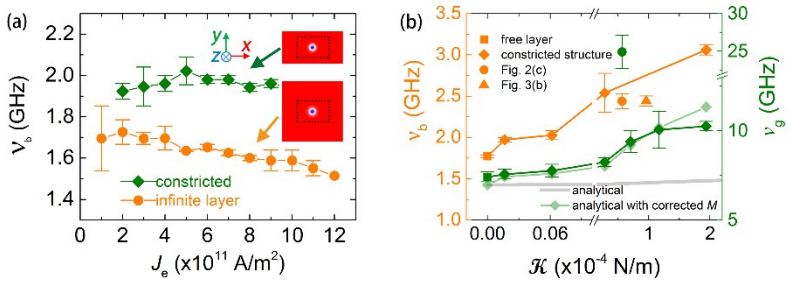

Supplementary Fig. 7 (a) Breathing mode frequency as a function of charge current density for a skyrmion in an infinite layer (orange circles) and in a racetrack with the width of $D_w = 160\ nm$ (green diamonds). (b) Stiffness K-dependent frequency of gyration and breathing modes. Square dots are data for a skyrmion in an infinite layer, and the diamond dots are data for a skyrmion in a racetrack. The grey line is calculated from the Eq. (S6) with a fixed inertial mass. The light green diamond dots are calculated from the Eq. (S6) with the corrected mass with the assumption that the mass density is a constant.

References

1. F. Büttner, I. Lemesh, M. Schneider, B. Pfau, C. M. Günther, P. Hessing, J. Geilhufe, L. Caretta, D. Engel and B. Krüger, *Nat. Nanotech.*, 2017, **12**, 1040.
2. P. Dürrenfeld, Y. Xu, J. Åkerman and Y. Zhou, *Phys. Rev. B*, 2017, **96**, 054430.
3. M.-W. Yoo, V. Cros and J.-V. Kim, *Phys. Rev. B*, 2017, **95**, 184423.
4. K. Litzius, I. Lemesh, B. Krüger, P. Bassirian, L. Caretta, K. Richter, F. Büttner, K. Sato, O. A. Tretiakov and J. Förster, *Nat. Phys.*, 2017, **13**, 170.